Chemical Compatibility and Reaction-Induced Exfoliation in Photopolymerizable Clay Nanocomposites

Kwame Owusu-Adom and C. Allan Guymon*

Department of Chemical & Biochemical Engineering, University of Iowa, 4133 Seamans Center, Iowa City, Iowa 52241

Received July 26, 2008; Revised Manuscript Received October 29, 2008

ABSTRACT: Exfoliation of clay nanoparticles is a critical step in achieving unique properties associated with clay−polymer nanocomposites. However, a rational means of designing exfoliated nanocomposites, especially in photopolymerizable systems, remain elusive to date. This study investigates the influence of monomer−clay dispersant interactions on organoclay dispersion behavior in photopolymerizable systems. The dispersion behavior of a nonpolar, nonpolymerizable organoclay in a range of monomers with different sizes and polarity was investigated utilizing X-ray scattering and electron microscopy. Results show that increasing chemical similarity between monomer and organoclay dispersant as well as enhanced polar/nonpolar interaction facilitates exfoliation. Organoclays modified with nonpolar dispersants only intercalates in polar polymers. Conversely, exfoliation of the nonpolar organoclay is facilitated in increasingly nonpolar polymers. A set of quaternary ammonium surfactants modified with methacrylate or thiol functionalities were used as dispersants for new organoclays. These polymerizable organoclays exfoliate more readily in a number of monomer systems as compared to nonpolymerizable organoclays. For polymerizable organoclays, the position of the reactive functional group and the type of functionality influence the degree of exfoliation. Methacrylate functionalized organoclays in which the reactive moiety is located away from the clay surface exfoliates before photopolymerization. Thiol functionalized organoclays disperse in a mixture of intercalated and exfoliated domains but exfoliate to a larger degree due to copolymerization of thiol and acrylate species in the clay galleries. Polymerizable organoclay systems exhibit higher storage modulus, glass transition temperatures, and enhanced photopolymerization behavior when compared to the nonpolymerizable analogues.

Introduction

Since the discovery of remarkable improvements in physical properties of polymeric materials with addition of small amounts of clay,[1−3] researchers have placed heavy emphasis on the synthesis of polymer−clay nanocomposites.[4−6] Such enhancements in properties have been attributed to the nanoscale dimensions of clay particles which allow significant polymer−clay interaction. Many unique aspects including improved mechanical, flame retardancy, and gas barrier properties have been observed in recent years.[4−9] The most significant enhancements have been observed with complete delamination of the clay platelet (exfoliation). The clay particles may also disperse in aggregates that retain their ordered morphology (intercalated state) with polymer embedded between clay layers. The most frequently observed morphology is a mixture of intercalated and exfoliated domains. To aid clay dispersion and exfoliation in organic media, hydrophilic clay particles are typically modified with quaternary ammonium surfactants.

Even with incorporation of quaternary ammonium surfactants, complete exfoliation of clay particles is usually difficult. Different mechanical and chemical means have been utilized to facilitate exfoliation to varying degrees of success. Exfoliated nanocomposites have been produced through application of shear force over long periods in melt-blended clay nanocomposites[10−13] as well as through solvent-aided exfoliation.[14,15] Other novel techniques have examined chemically induced delamination through surface-initiated polymerization techniques.[16,17] Initiating polymerization from clay surfaces allows growth of polymer that could aid exfoliation as the polymer chains grow in size, breaking apart the clay aggregates. To date, no substantive approach has been successfully utilized to exfoliate clays in different systems. Since the ability to induce exfoliation depends on interactions between monomer and organoclay surface, especially for systems formed in situ, a fundamental understanding of this relationship is important to successfully design exfoliated nanocomposite materials. It would be expected, for instance, that clay particles would exfoliate more readily in systems in which the clay surface modifiers are chemically similar to the monomer. This premise is indeed the principal reason for utilizing dispersants in organoclay−polymer composite systems. Hence, understanding such interactions is important to the design of exfoliated nanocomposite systems that could access advanced properties not attainable with traditional composites.

While such knowledge could be useful in designing exfoliated nanocomposites in thermoplastic materials obtained through melt-blending or solvent-induced processing, it is especially critical in developing cross-linked polymer materials. Nanocomposites formed by in situ processes such as photopolymerization are at a disadvantage since network formation occurs rapidly, thus limiting monomer diffusion into clay galleries that would aid exfoliation. On the other hand, photopolymers are an important class of materials that may benefit significantly from the novel properties imparted by nanoparticles. Photopolymerization continues to expand rapidly due to unique advantages such as ultrafast reactions, solvent-free reaction media, and temporal and spatial control of initiation.[18] Decker et al. and others have successfully developed clay photopolymer materials with some enhancement in properties.[6,7,19] However, few studies have investigated the impact of constituent interactions in order to optimize the nanocomposite properties through clay particle exfoliation.

The lack of information regarding photopolymerizable nanocomposites may also be a result of potential difficulties in generating exfoliated nanoclays due to the photopolymerization mechanism. The degree to which clay particles exfoliate in a

* Corresponding author: Ph 319-335-5015; Fax 319-335-1415, e-mail cguymon@engineering.uiowa.edu.

10.1021/ma801688q CCC: $40.75
Published on Web 12/10/2008

monomer system depends largely on swelling and delamination of clay particles by the monomer before polymerization. Delamination of the clay aggregates may also occur through formation of larger polymer chains that breaks the aggregates apart to generate exfoliated domains during polymerization.[20] The inherent speed of photopolymerization may necessitate control of the original organoclay dispersion in the monomer since highly cross-linked networks quickly form upon initiating polymerization in most photopolymer systems. For example, gelation of multifunctional acrylates during photopolymerization occurs at very low conversion levels.[21,22] Hence, potential clay delamination during photopolymerization could be hindered significantly and reduce the potential for exfoliation. A means of circumventing this problem could be developed from understanding the influence of dispersant−monomer interactions on clay dispersion behavior in photopolymerizable systems.

In this study, the dispersion behavior of organoclays in photopolymerizable monomers with different chemical structure and properties is examined with the objective of determining the effect of chemical interactions on organoclay dispersion. In particular, the effects of monomer chemical structure and size on clay dispersion mechanism in photopolymerizable systems are investigated. Understanding gained from this study is used to develop organoclay systems with potential for improved dispersion in different photopolymerizable formulations. These organoclays were designed based on the premise that dispersants with similar chemical characteristics as the monomer would interact more readily to facilitate exfoliation. Hence, dispersants that have polymerizable moieties similar to the monomers used in this study were investigated. The influence of the type of dispersant on dispersion, thermomechanical properties, and photopolymerization kinetics is examined. Effects of the position of the reactive moiety in the polymerizable dispersant as well as the type of reactive functionality in the organoclays are also investigated.

Experimental Section

Materials. Cloisite 15A (Southern Clay Products, Gonzales, TX) was utilized to examine the influence of the type of dispersant on organoclay dispersibility in different monomers. Cloisite 15A, a natural montmorillonite clay modified with a dihydrogenated tallow, HT (HT = ∼65% C18, ∼30% C16, ∼5% C14), was first investigated. The dihydrogenated tallow renders CL15A quite nonpolar. A pristine clay (Cloisite Na, Southern Clay Products, CEC = 92.6 mequiv/100 g clay) was used to form the polymerizable organoclays. Two of the polymerizable surfactants used for clay surface modification are based on quaternary ammonium surfactant structures modified with methacrylate functionalities. Tetradecyl-2-methacryloyloxy(ethyl)dimethylammonium bromide (C14MA) and undecylmethacryloyloxytrimethylammonium bromide (PM1), the two types of methacrylate-modified quaternary ammonium surfactants used, were synthesized as described elsewhere.[23,24] Organoclays bearing these dispersants were produced following typical cation exchange procedures and will be referred to as C14MA−organoclay and PM1−organoclay, respectively.[25] A third organoclay, PSH2−organoclay, was synthesized by reacting a multifunctional thiol monomer into an acrylate analogue of C14MA−organoclay through amine-catalyzed reaction of C14A and trimethylol tris(3-mercaptopropionate) as described below. Poly(ethylene glycol) diacrylate (PEGDA, M_n = 575), tripropylene glycol diacrylate (TrPGDA), and neopentyl glycol diacrylate (NPGDA) were the monomers used in addition to 1,6-hexanediol diacrylate (HDDA) and tridecyl acrylate (trdA). All monomers were obtained from Sartomer and used as received. Photopolymerization reactions were initiated by 365 nm light using 0.1 wt % 2,2-dimethoxyphenylacetophenone (DMPA, Ciba) at 3 mW/cm^2. Trimethylolpropane tris(3-mercaptopropionate) (trithiol), tetrahydrofuran (THF), diethylamine, and methanol used for synthesizing PSH2 surfactant were obtained from Sigma Aldrich. Figure 1 shows

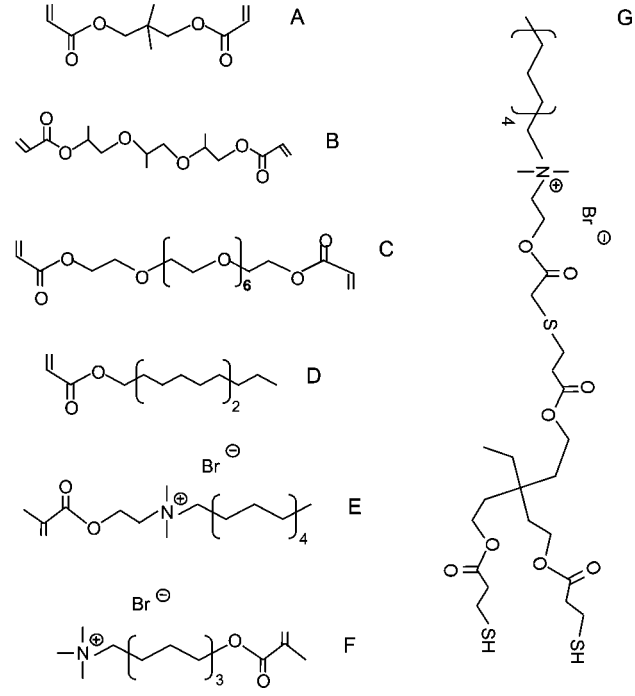

Figure 1. Chemical structures of monomers and organic modifiers used: (A) neopentylglycol diacrylate (NPGDA), (B) tri(ethylene glycol) diacrylate (TrPGDA), (C) poly(ethylene)glycol diacrylate (PEGDA), (D) tridecyl acrylate (trdA), (E) undecylmethacryloyloxytrimethylammonium bromide (PM1), (F) tetradecyl-2-methacryloyloxy(ethyl)-dimethylammonium bromide (C14MA), and (G) tetradecyltrimethylolbis(3-mercaptopropionate)dimethylammonium bromide (PSH2).

chemical structures of the surfactants and monomers used in this study.

Methods. PSH2−organoclay was synthesized from an acrylated C14MA−organoclay according to the following procedure. To a round-bottom flask was added 5 g of the acrylated C14MA−organoclay and 50 mL of THF. The mixture was stirred continuously for 30 min followed by 1 h sonication to aid clay dispersion. After cooling the mixture, excess thiol (5 g total) was added to the mixture and stirred for another 30 min. Diethylamine (0.5 mol %) was added dropwise to the mixture and stirred continuously at room temperature for 12−24 h. The mixture was separated by a centrifuge and washed several times with THF. The resulting organoclay product was freeze-dried and characterized for presence of thiol functional groups using Fourier transform infrared spectroscopy (FTIR, Nexus 670 IR).

Small-angle X-ray scattering (SAXS) was utilized to characterize organoclay dispersion behavior in the different monomers. These measurements were conducted using a Nonius FR590 X-ray apparatus equipped with a Cu Kα radiation source (λ = 1.54 Å) at 40 kV and 30 mA intensity.[26] Transmission electron microscope (TEM) images were collected with JEOL JEM 1230 TEM operated at 120 kV. Approximately 100 nm thick samples were microtomed (Leica UC6 Ultramicrotome) onto 400 mesh copper grids for imaging. Cryo-TEM sections were collected after samples were cooled to −170 °C. Rectangular bars measuring approximately 2 × 13 × 25 mm were fabricated for analyzing glass transition temperatures, Young's moduli, and storage moduli of samples using a dynamic mechanical analysis instrument (DMA-Q800, TA Instruments). Young's modulus measurements were taken at 30 °C with an applied dynamic force in the linear regime (typically less than 5% strain). All DMA experiments were performed in tension mode and with the average of at least three test results reported. Photopolymerization behavior was monitored using a Perkin-Elmer Diamond differential scanning calorimeter modified with a medium pressure mercury arc lamp (photo-DSC). Photopolymerization rate was directly determined from the heat released as recorded by photo-DSC.[27] The rates of photopolymerization reported are

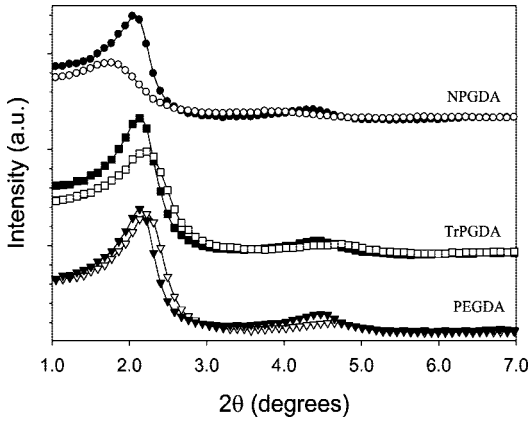

Figure 2. SAXS profiles of 3 wt % Cloisite 15A in NPGDA, TrPGDA, and PEGDA. Unpolymerized samples are shown with filled symbols while unfilled symbols represent polymerized samples.

normalized to the concentration of reactive species in the sample to ensure equal basis of comparison.

Results and Discussion

Dispersion of Nonreactive Organoclay. Photopolymers are used in a number of applications that may benefit from the unique property enhancement afforded by nanoparticulate fillers. The extent to which these unique properties can be realized likely will depend on the ability to exfoliate clay aggregates into their nanoscale dimensions. However, because of the ultrafast nature of photopolymerization reactions, generating exfoliated clay platelets before polymerization may be necessary to prevent clay aggregates from being trapped within the cross-link network. Achieving this state requires that an understanding of monomer−dispersant interactions, and their effect on organoclay dispersion is gained. It would be expected that the interaction between the organoclay surface modifier and the type of monomer/oligomer significantly influences the extent of exfoliation since organoclay swelling by monomer is a necessary precursor to exfoliation for materials formed in situ.

To investigate this phenomenon, the dispersion of a nonpolar organoclay in a series of photopolymerizable acrylate monomers with different molecular size and polarity were studied via SAXS. NPGDA, TrPGDA, and PEGDA are difunctional acrylate species with increasing size and polarity while HDDA and trdA are representative nonpolar monomers used. These monomers were used to examine the effects of polar/nonpolar monomer interactions with the nonpolar organoclay dispersants. Small-angle X-ray scattering profiles of the dispersion behavior of CL15A in NPGDA, TrPGDA, and PEGDA are shown in Figure 2. The X-ray profiles have been offset to facilitate comparison of the dispersion profiles. HT-modified CL15A has a *d*-spacing of 3.15 nm (corresponding to $2\theta = 2.8°$ according to the supplier) before it is added to the monomer. A prominent peak centered on 2.1° appears in the CL15A−NPGDA system before photopolymerization which indicates an intercalated morphology. The peak intensity decreases and shifts to smaller angles after polymerization and indicates an increase in *d*-spacing, while the lowered peak intensity suggests formation of more disordered domains in the organoclay. The peak appears more defined before polymerization when CL15A is dispersed in TrPGDA (Figure 2). No significant changes in the peak intensity occur, and the peak shifts to slightly higher 2θ after polymerization. This behavior shows that CL15A is intercalated before photopolymerization and remains so with a slight decrease in the *d*-spacing after photopolymerization. Similar *d*-spacing is observed in both NPGDA− and TrPGDA−CL15A systems before photopolymerization, indicating that the organoclay swells to approximately the same extent in both monomers. The contrast in dispersion behavior is more evident when the SAXS profiles of the polymerized samples are compared. While CL15A exhibits larger *d*-spacing after polymerization of NPGDA, no significant change in *d*-spacing is observed in the TrPGDA−organoclay system.

In comparison, SAXS of CL15A in PEGDA shows a prominent peak before and after polymerization. The peak is centered on similar 2θ values as observed in both NPGDA and TrPGDA systems before polymerization and remains similar to that of the TrPGDA system afterward. Photopolymerizing the sample yields intercalated organoclay morphology with a slight decrease in the *d*-spacing. While SAXS is useful for characterizing changes in apparent interlayer spacing, it is often inadequate to determine exfoliation in nanocomposites. Electron microscopy techniques are typically used to corroborate SAXS studies. TEM images of the polymerized samples shown in Figure 3 indicate that CL15A intercalates to some degree in all three polymer systems. However, CL15A disperses into smaller sized aggregates in NPGDA (Figure 3a) compared to either aggregates in TrGPDA (Figure 3b) or PEGDA (Figure 3c) polymers and agrees with the SAXS data. On average, aggregate sizes of approximately 7, 17, and 20 nm are observed for CL15A in NPGDA, TrPGDA, and PEGDA polymers, respectively. From these studies, it can be seen that monomer size plays a lesser role in the dispersion of nonpolar organoclay in polar monomers. The changes in *d*-spacing of CL15A dispersed in PEGDA are similar to the TrPGDA system but markedly different from NPGDA after photopolymerization. While *d*-spacing decreases or remains the same in both TrPGDA and PEGDA after photopolymerization, a larger *d*-spacing is observed for the organoclay dispersed in NPGDA. In addition, there appears to be some disordering of the clay morphology in NPGDA but little in either TrPGDA or PEGDA polymer systems. This suggests that the nature of monomer plays an important role in retaining polymer in the clay galleries during photopolymerization.

When clay is dispersed in the more hydrophobic NPGDA, a greater number of polymer chains appear to be localized between the clay galleries which lead to larger *d*-spacing after photopolymerization. This behavior is not observed in either the TrPGDA− or PEGDA−organoclay systems as no significant changes occur to the diffraction peaks during photopolymerization. Since differences in the nature of the monomers and dispersants are obviously important, comparing the dispersion profiles of CL15A in NPGDA to TrPGDA and PEGDA suggests that increasing the polarity of the monomer leads to more intercalated and less exfoliated domains. Since increasing the monomer polarity appears to lead to the formation of intercalated composites, the dispersion behavior of CL15A in monomers with increasing polarity and greater chemical similarity to the dispersant was investigated to better understand the influence of dispersant−monomer interactions on organoclay dispersion.

To examine the influence of nonpolar interactions on organoclay dispersion, two monomers with increasing aliphatic component (HDDA and trdA) were studied in combination with CL15A. The SAXS dispersion profiles of 3 wt % CL15A in HDDA and trdA are shown in Figure 4 along with NPGDA for comparison. A diffraction peak centered on ∼1.5° is observed for CL15A dispersed in HDDA before photopolymerization. The peak intensity decreases significantly after photopolymerization to indicate disruption of the organoclay domains. With an even larger aliphatic component in trdA monomer, the peak intensity decreases substantially before photopolymerization. The morphology of CL15A appears to be disrupted even more in trdA after photopolymerization and appears to exfoliate more easily in the nonpolar monomers from the SAXS profiles. Even with

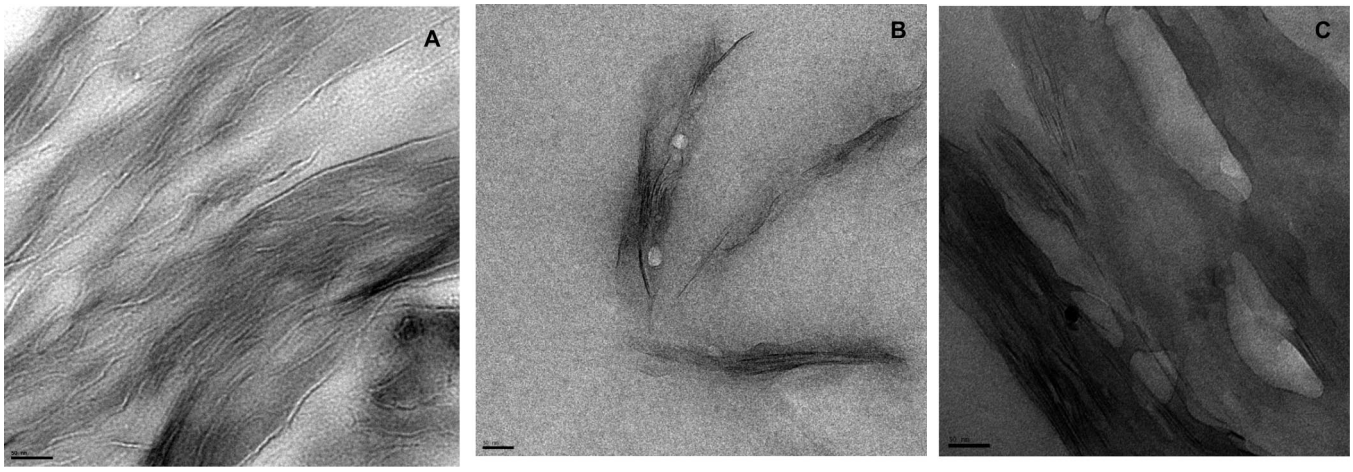

Figure 3. TEM of 3 wt % Cloisite 15A in NPGDA (A), TrPGDA (B), and PEGDA (C). Scale bar is 50 nm.

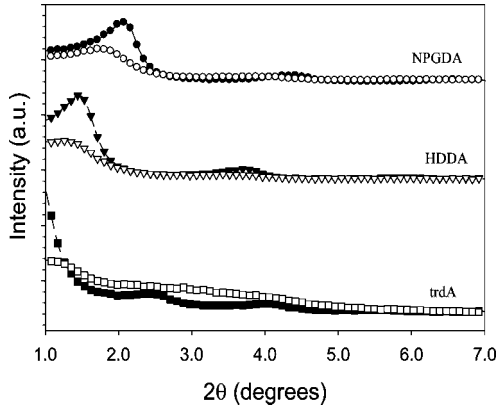

Figure 4. SAXS profiles of 3 wt % Cloisite 15A in NPGDA, HDDA, and trdA. Uncured samples are shown with filled symbols. Unfilled symbols represent polymerized samples.

this evidence of exfoliation, TEM images show that CL15A does form some aggregates in HDDA and trdA (Figure 5a). The domain sizes of CL15A in HDDA appear much smaller (approximately 2−3 nm aggregate sizes), however, in comparison to TrGPDA samples shown in Figure 3. The aggregate sizes reduce further in trdA when CL15A is dispersed in the polymer matrix as Figure 5b shows. These results also indicate that CL15A swells more in HDDA than NPGDA. Further, when monomer polarity is varied, completely different dispersion behaviors occur as evidenced by the contrast between HDDA and TrPGDA systems. While the peak in CL15A−HDDA decreases after photopolymerization, the CL15A−TrPGDA remains unchanged. The dispersion behavior in these monomers shows that decreasing the polarity of the monomer and increasing the similarity to the dispersant enhances exfoliation of the nonpolar CL15A, while more polar monomers lead to intercalated organoclay aggregates.

From the above results, it is clear that choosing monomers/oligomers that are chemically compatible (based on structural similarities and polarity) with a particular organoclay enhances the ability to fabricate photopolymer nanocomposites with exfoliated organoclay. Though the results show a systematic basis for choosing organoclays for different photopolymerizable systems, application of this technique severely limits one's ability to utilize certain organoclays in different oligomer/polymer materials. A more versatile approach for developing photopolymer−clay nanocomposites would be one in which the organoclay is designed to be compatible with the monomer and not vice versa. One means of achieving this goal could be modification of the dispersant chemistry.

Dispersion Behavior of Polymerizable Organoclays. Modifying dispersant chemistry provides distinct advantages over other techniques. For photopolymerizable (meth)acrylate systems, similar (meth)acrylate functionalities can be introduced into quaternary ammonium surfactants to be used for organic modification.[23,24] Methacrylate functional groups may increase dispersant compatibility with (meth)acrylate monomers based on similarities in organoclay and monomer functionalities. Hence, various polymerizable organoclays were developed by first synthesizing methacrylated (C14MA and PM1) and thiol (PSH2) quaternary ammonium surfactants and modifying clay surfaces through typical cation exchange procedures. C14MA− and PM1−organoclays are methacrylate-functionalized organoclays in which the polymerizable functional groups are located at different positions with respect to the cationic ammonium head. The functional group is located close to the cationic head of the surfactant in C14MA. In PM1−organoclay, the reactive functionality is located at the end of the aliphatic chain and is potentially more accessible to intragallery species.

Because these dispersants and interlayer monomer should copolymerize inside the clay galleries, the large intragallery polymer chains formed could be utilized to aid exfoliation (Scheme 1). The effectiveness of such a technique could be further investigated by utilizing monomers with certain preferential polymerization behavior. Photopolymerization based on thiol and acrylate species exhibit unique properties compared to pure (meth)acrylate polymerizations. An important consideration for this study is that thiol monomers do not homopolymerize but do copolymerize readily with acrylate species.[28−30] In a thiol−acrylate mixture, homopolymerization of acrylate free radicals occur along with chain transfer to or hydrogen abstraction from the thiol, leading to propagation and a thiol−acrylate copolymer network. Therefore, modifying clay surfaces with thiol functional groups could be a useful tool for probing exfoliation behavior induced by apparent intragallery polymerization. In this way, PSH2−organoclay may help to elucidate the influence of reactive functional groups on the ability to exfoliate organoclay during photopolymerization. The dispersion behavior of these polymerizable organoclays in HDDA and PEGDA was examined via SAXS. The SAXS profiles of 3 wt % polymerizable organoclay in HDDA are shown in Figure 6 along with TEM images of these systems in Figure 7.

Before photopolymerizing C14MA−organoclay in HDDA, the SAXS profile shows a broad diffraction peak centered at ∼2.2°. The peak intensity decreases after polymerization but does not show any appreciable change in the *d*-spacing. Compared to C14MA−organoclay, the PM1−organoclay/

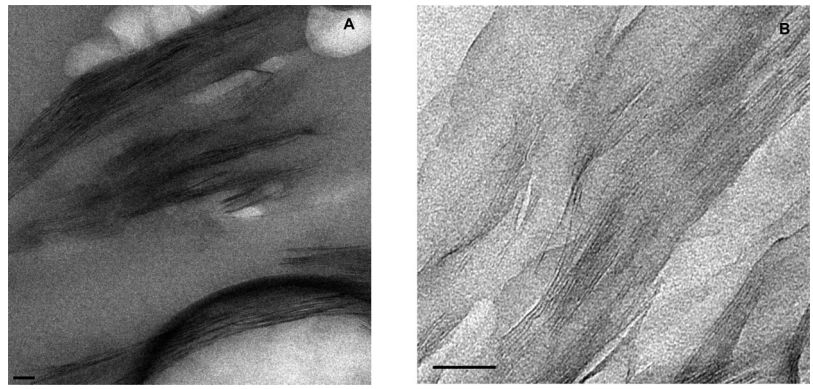

Figure 5. TEM of 3 wt % Cloisite 15A in HDDA (A) and trdA (B). Scale bar is 50 nm.

Scheme 1. Schematic of Monomer Diffusion into Organoclay Interlayer

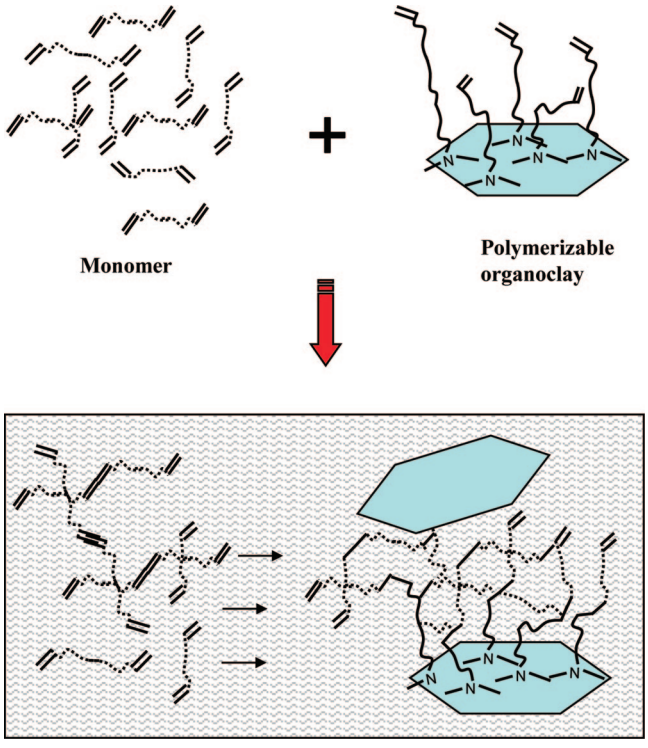

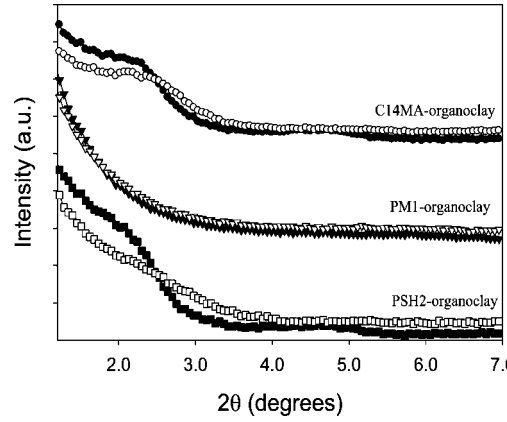

Figure 6. SAXS profiles of 3 wt % C14MA−organoclay, 3 wt % PM1−organoclay, and 3 wt % PSH2−organoclay in HDDA. Prepolymerized samples represented by filled symbols. Empty symbols indicate polymerized samples.

HDDA sample appears extensively exfoliated before photopolymerization. No diffraction peak is observed in the SAXS profile that would indicate an intercalated morphology. PSH2−organoclay, on the other hand, appears to intercalate to a small degree in HDDA before photopolymerization. Upon photopolymerization, the primary peak practically disappears, suggesting that the ordered morphology of the clay platelets is largely disrupted. The trends in the dispersion behavior observed via SAXS are supported by TEM micrographs in Figure 7. Figure 7A shows that C14MA−organoclay is intercalated in HDDA with relatively large aggregates in the polymer. The dispersion improves significantly for PM1−organoclay for which individually separated clay platelets (ca. 2−3 nm domain sizes) appear with limited ordered morphology. The PSH2−organoclay system shows some exfoliated domains along with intercalated aggregates. The distinct differences in dispersion behavior observed in the three types of organoclays are induced by the chemical structure and reactivity.

Because of the proximity of the methacrylate functionality to the clay surface in C14MA−organoclay, steric hindrance from the aliphatic tail may decrease the organoclay compatibility with HDDA. This shielding mechanism may lead to an effectively nonpolar interlayer which lowers monomer association with dispersants in a similar manner as observed in the CL15A system. The location of the polymerizable group in PM1−organoclay results in a different dispersion dynamic. The polymerizable moiety is more accessible to intragallery monomer because it is located away from the clay surface. Hence, steric effects preventing interactions such as those observed in C14MA−organoclay are significantly reduced. Second, accessibility to the methacrylate functional group may increase compatibility between the polar methacrylate ends and the acrylate groups of HDDA. Such interactions are consistent with the observed dispersion of PM1−organoclay in HDDA even before photopolymerization. Introducing the polymerizable group then creates a more favorable environment for greater monomer compatibility in the clay galleries, as observed in Figures 6 and 7. For the PSH2−organoclay system, the significant morphological disruption could be due to the nature of the interactions between acrylate and thiol monomer in the galleries. Since the thiol functional group only reacts with the interlayer HDDA, the resulting copolymer chains induce further disruption of the organoclay. In addition, depletion of intragallery HDDA monomer during the reaction may facilitate continuous monomer diffusion into the galleries. This enables more polymer formation within the clay interlayers and may lead to the observed dispersion profiles.

Dispersion of the polymerizable organoclays was also examined in larger molecular weight and more polar monomers such as PEGDA. 3 wt % C14MA−, PM1−, and PSH2−organoclay dispersed in PEGDA was investigated via SAXS with results shown in Figure 8. A significant primary peak is observed in

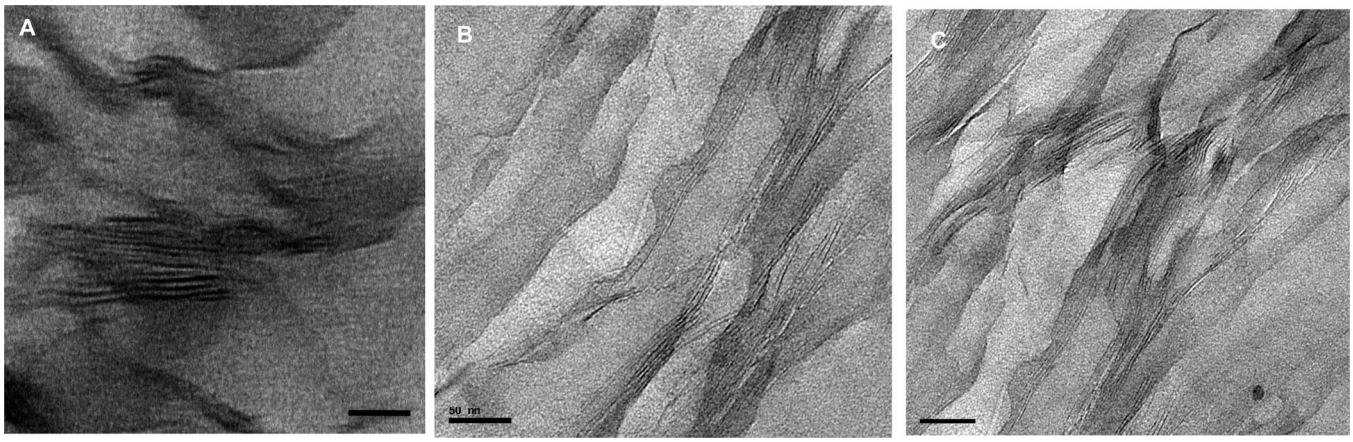

Figure 7. TEM of 3 wt % C14MA−organoclay (A), 3 wt % PM1−organoclay (B), and 3 wt % PSH2−organoclay (C) dispersed in HDDA polymer. Scale: 50 nm.

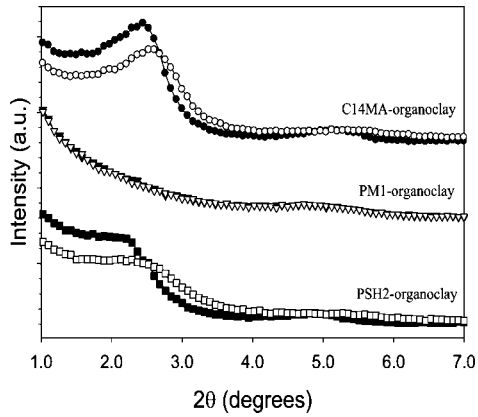

Figure 8. SAXS profiles of 3 wt % C14MA−organoclay, 3 wt % PM1−organoclay, and 3 wt % PSH2−organoclay in PEGDA. Prepolymerized samples are represented by filled cells. Unfilled cells indicate polymerized samples.

the SAXS profile of C14MA−organoclay before photopolymerization. The intercalated sample exhibits smaller *d*-spacing after photopolymerization. On the other hand, no primary peak is observed in the PM1−organoclay profile both before and after photopolymerization. The intercalated morphology of PSH2−organoclay is significantly disrupted as evidenced by the broad peak before polymerization. The peak intensity decreases after photopolymerization, but the sample appears to remain intercalated. TEM micrographs in Figure 9A−C corroborate results from SAXS experiments. C14MA− and PSH2−organoclays systems are intercalated with similar dispersion of the organoclay aggregates (Figure 9A,C). Some exfoliated domains in the PSH2−organoclay samples are apparent which could lead to the diffused peak observed in Figure 8. All of the polymerizable organoclays disperse in a completely different fashion compared to the nonpolymerizable organoclay systems. While CL15A intercalates into PEGDA before and after photopolymerization, PM1−organoclay appears exfoliated. PSH2−organoclay shows some amount of exfoliation while C14MA−organoclay is intercalated. Even in the intercalated state, TEM shows that the domain size of C14MA−organoclay appears smaller compared to CL15A dispersed in PEGDA. The copolymer formed from reacting thiol dispersants with the acrylate monomer could lead to the dispersion behavior observed for PSH2−organoclay in a similar fashion as observed in the NPGDA system. The smaller interlayer spacing after photopolymerizing C14MA−organoclay in PEGDA may in part be due to polymerization-induced shrinkage, typical in the photopolymerization of acrylate systems.[21,22]

Photopolymerization Kinetics and Physical Properties. To probe the influence of the extent of intercalation/exfoliation morphologies on mechanical properties of these photopolymer nanocomposites, dynamic mechanical analysis (DMA) was used to examine the storage and Young's moduli of the nanocomposites. Storage modulus as a function of temperature for 5 wt % organoclay dispersed in HDDA is shown in Figure 10, and Table 1 shows the Young's modulus of 3 wt % organoclay−PEGDA samples. The CL15A−HDDA polymer system has a storage modulus that is ∼30% lower than the neat polymer. At room temperature, the storage modulus of poly(HDDA) containing either C14MA− or PM1−organoclay systems is 30−35% higher than the unfilled polymer, while adding the poly(HDDA) sample containing PSH2−organoclay has approximately double the storage modulus of the neat polymer. The storage modulus remains higher than the neat polymer even at temperatures above 100 °C. In addition, even in the intercalated state, the polymer containing C14MA−organoclay exhibits similar storage modulus as the exfoliated PM1−organoclay system. This behavior could be due to significant interactions between organoclay and polymer chains since the functionalized organoclay can polymerize into the overall network. CL15A−poly(HDDA), on the other hand, exhibits lower modulus possibly because of disruption of the polymer cross-link network as well as inhomogeneities induced by the larger clay aggregates.

Adding organoclay to PEGDA changes the mechanical properties in a much different way. Approximately 30−35% increase in the Young's modulus at room temperature results from adding only 3 wt % of the polymerizable organoclays to PEGDA. PEGDA polymers containing PM1−organoclay are slightly more mechanically stable than that containing C14MA−organoclay at room temperature which could be related to the more extensive dispersion behavior observed. In comparison, adding 3 wt % CL15A increases the modulus by only 10%. It is noteworthy to mention that even though both CL15A and C14MA−organoclay intercalate in PEGDA, the reactive functionality induces greater changes in the mechanical properties of the nanocomposite due to copolymerization of the organoclays with the bulk polymer network.

Further DMA studies were conducted to investigate the effects of dispersed organoclay on nanocomposite thermal properties. Figure 11 shows tan δ curves as a function of temperature for 3 wt % organoclay in PEGDA. The temperature at the peak of the tan δ curve is used as a measure of T_g.[31] A slight increase in glass transition temperature is observed when CL15A is incorporated while C14MA−organoclay addition results in a significantly higher T_g (∼5 °C increase). The increase in T_g observed in Figure 11 can be attributed to several factors. Even

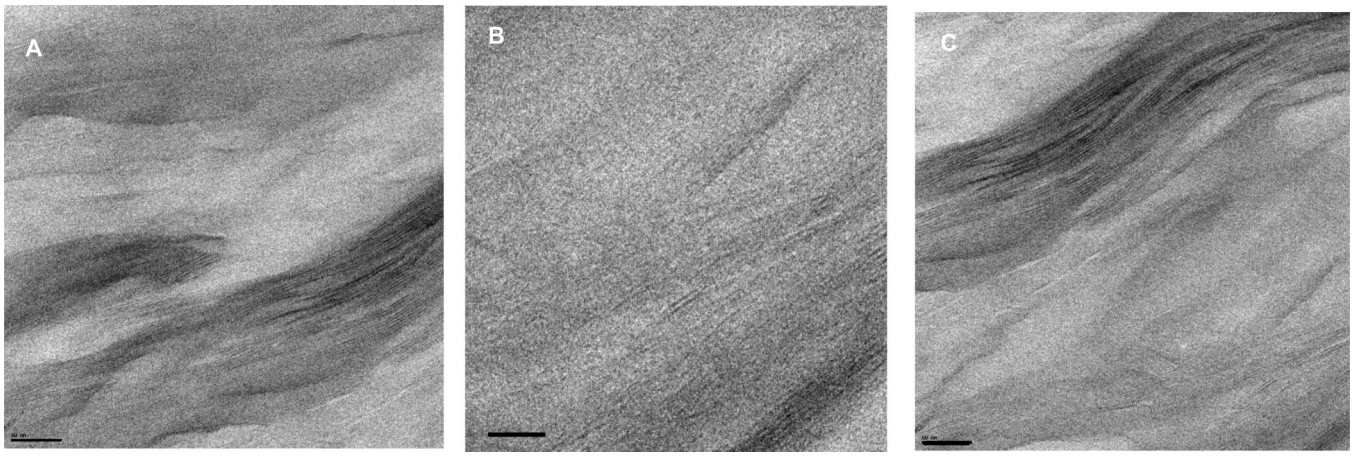

Figure 9. TEM of 3 wt % C14MA−organoclay (A), 3 wt % PM1−organoclay (B), and 3 wt % PSH2−organoclay (C) in PEGDA. Scale: 50 nm.

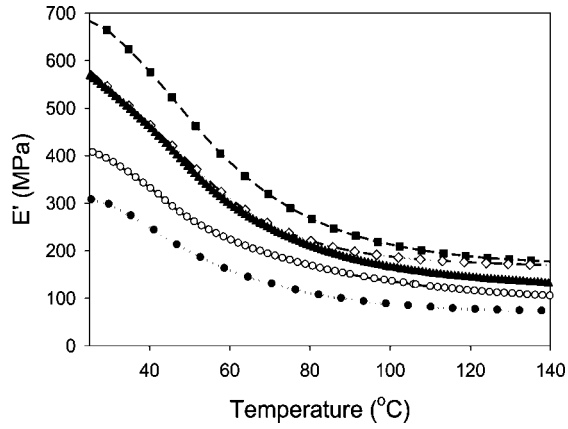

Figure 10. Storage modulus as a function of temperature for 5 wt % Cloisite 15A (●), C14MA−organoclay (▼), PM1−organoclay (◇), and PSH2−organoclay (■) dispersed in HDDA. Unfilled polymer (○) is shown for comparison.

Table 1. Young's Modulus of 3 wt % Organoclay in PEGDA at 30 °C

monomer	organic modifier	Young's modulus (MPa)
PEGDA	none	43 ± 4
	CL15A	48 ± 2
	C14MA−organoclay	56 ± 4
	PM1−organoclay	58 ± 2
	PSH2−organoclay	52 ± 2

in the intercalated state, dispersed CL15A particles could limit mobility of polymer chains due to caging effects as described by Rao et al.[32] The enhanced compatibility between monomer and C14MA−organoclay as well as copolymerization of C14MA with the polymer network lead to further reduction in polymer chain mobility and a corresponding increase in T_g.

A potential limitation of incorporating clay particles into photopolymerizable systems may be reduction in polymerization rates observed in filled systems.[19,33] To examine the influence of polymerizable organoclays on photopolymerization behavior, photodifferential scanning calorimetry was used to evaluate photopolymerization rates as a function of organoclay concentration. Figure 12 shows the rate of photopolymerization of various organoclays in PEGDA and HDDA as determined by photo-DSC. The rate of photopolymerization as a function of conversion for 3 wt % organoclay in PEGDA is shown in Figure 12a. As expected, addition of organoclay leads to rate decreases most likely due to light scattering and absorption by the organoclay particles. Similar rates of photopolymerization are

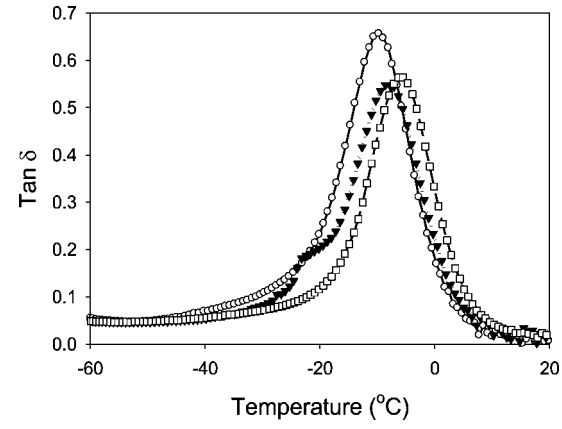

Figure 11. Tan δ vs temperature plot of 3 wt % Cloisite 15A (▼) and C14MA−organoclay (□) in PEGDA (○).

observed in all the PEGDA/organoclay samples.. The rate of photopolymerization of the filled formulations is ∼30% lower than the neat system. Higher double bond conversion is also observed in the neat polymer in relation to the filled formulations.

In comparison to the PEGDA−organoclay system, blending organoclay into HDDA leads to completely different photopolymerization behavior. Figure 12b shows percent change in the maximum rate of photopolymerization as a function of the type of organoclay and concentration. Increasing the amount of organoclay generally decreases the rate of photopolymerization. For a nonpolymerizable organoclay, a monotonic decrease in maximum rate of polymerization occurs with higher organoclay concentration. Incorporating a reactive functionality changes this trend, as the maximum photopolymerization rate appears to plateau after an initial decrease in all the polymerizable organoclay systems. The thiol functionality appears to decrease photopolymerization rates to the least degree with a much lower overall decrease in the polymerization rate compared to polymers containing C14MA− and PM1−organoclay. The rate of photopolymerization is significantly enhanced in the presence of polymerizable organoclays in comparison to traditional nonpolymerizable organoclay formulations.

The enhanced rate observed in the polymerizable organoclay systems is most likely due to the nanosized clay domains resulting from increasing the amount of exfoliated clay particles that lower light scattering in the formulation. In addition, the presence of the anchored polymerizable functionalities may decrease bimolecular termination, which leads to higher polym-

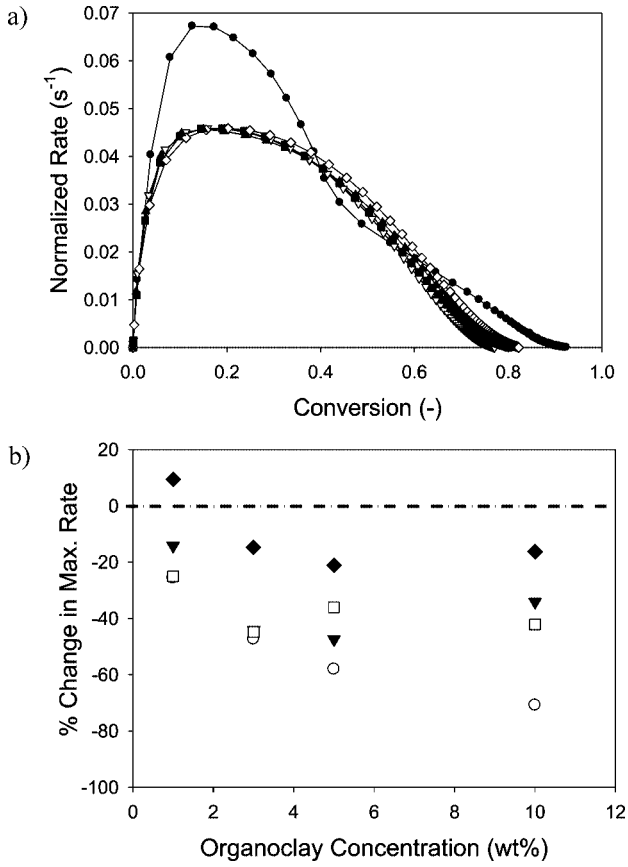

Figure 12. (a) Normalized rate of photopolymerization as a function of conversion for 3 wt % Cloisite 15A (Δ), C14MA−organoclay (■), PM1−organoclay (◇), and PSH2−organoclay (▲) in PEGDA. Samples contain 0.1 wt % DMPA and were irradiated with 3 mW/cm^2. Neat PEGDA (●) is shown for comparison. (b) Change in maximum rate of photopolymerization as a function of organoclay type and concentration for TTAB (○), C14MA (▼), PM1 (□), and PSH2−organoclays (◆) dispersed in HDDA. Percent change indicates deviation from the rate of polymerization of the unfilled HDDA (dashed line). Samples contain 0.1 wt % DMPA and were irradiated with 365 nm light at 3 mW/cm^2.

erization rates as observed in other systems.[19,34−36] Such mechanisms have been demonstrated in other templated polymerizations.[34,38]

Conclusions

This study explores the effects of organoclay dispersant and monomer interaction on dispersion in photopolymer systems. The *d*-spacing of nonpolar organoclay/monomer systems increases with decreasing monomer polarity. Nonpolar organoclay aggregate sizes decrease significantly when dispersed in increasingly nonpolar monomer. On the contrary, dispersing the organoclay in polar monomer leads to intercalated materials. Enhanced dispersion is induced with increased chemical similarities between monomer and dispersant. Polymerization within clay galleries facilitates that allows further exfoliation. Organoclay dispersion is enhanced in different monomers when polymerizable methacrylate functionalities are incorporated into organoclays. Methacrylate functional groups located close to the clay surface result in intercalated organoclay domains with small aggregate sizes. When the reactive moiety is located away from the clay surface, creating a more accessible functional group, organoclay exfoliation occurs even before photopolymerization in a variety of monomers. Overall, similarities in the chemical nature of methacrylated organoclay dispersants and the monomer facilitate exfoliation. For thiolated organoclays, enhanced exfoliation occurs through copolymerization of thiol functional groups and acrylate monomer during photopolymerization. Incorporating reactive organoclays lead to higher moduli and T_g in the nanocomposites while also facilitating higher photopolymerization rates compared to nonpolymerizable analogues.

Acknowledgment. The authors acknowledge financial support from the National Science Foundation (CTS-0626395), the I/UCRC Center for Photopolymerization Fundamentals and Application, and a University of Iowa AGEP fellowship. Dr. Randy Nessler and the staff of Central Microscopy Research Facilities (CMRF) at the University of Iowa are gratefully acknowledged for help with TEM imaging.

References and Notes

(1) Okada, A.; Kawasumi, M.; Kurauchi, T.; Kamigaito, O. *Polym Prepr.* **1987**, *28*, 447–448.
(2) Okada, A.; Kawasumi, M.; Kurauchi, T.; Kamigaito, O. US Patent No. 4739007, **1988**.
(3) Okada, A.; Fukushima, A.; Kawasumi, M.; Inagaki, S.; Usuki, A.; Sugiyama, S.; Kurauchi, T. *Chem. Abstr.* **1987**, *107*, 60084.
(4) Alexandre, M.; Dubois, P. *Mater. Sci. Eng.* **2000**, *28*, 1–63.
(5) Vaia, R. A.; Giannelis, E. P. *Macromolecules* **1997**, *30*, 7990–7999.
(6) Decker, C.; Keller, L.; Zahouily, K.; Benfarhi, S. *Polymer* **2005**, *46*, 6640–6648.
(7) Usuku, A.; Kojima, Y.; Kawasumi, M.; Okada, A.; Fukushima, Y.; Kurauchi, T.; Kamigaito, O. *J. Mater. Res.* **1993**, *8*, 1185–1189.
(8) Okada, A.; Fukumori, K.; Usuki, A.; Kojima, Y.; Sato, N.; Kurauchi, T.; Kamigaito, O. *Polym. Prepr.* **1991**, *32*, 540–541.
(9) Uhl, F. M.; Davuluri, S. P.; Wong, S. C.; Webster, D. C. *Chem. Mater.* **2004**, *6*, 1135–1142.
(10) Tabtiang, A.; Lumlong, S.; Venables, R. A. *Polym.-Plast. Technol. Eng.* **2000**, *39*, 293–303.
(11) Huang, X. Y.; Brittain, W. J. *Macromolecules* **2001**, *34*, 3255–3260.
(12) Xie, W.; Gao, Z. M.; Pan, W. P.; Hunter, D.; Singh, A.; Vaia, R. *Chem. Mater.* **2001**, *13*, 2979–2990.
(13) Bhiwankar, N. N.; Weiss, R. A. *Polymer* **2006**, *47*, 6684–6691.
(14) Horsch, S.; Serhatkulu, G.; Gulari, E.; Kannan, R. M. *Polymer* **2006**, *47*, 7485–7496.
(15) Hasegawa, N.; Okamoto, H.; Kato, M.; Usuki, A.; Sato, N. *Polymer* **2003**, *44*, 2933–2937.
(16) Weimer, M. W.; Chen, H.; Giannelis, E. P.; Sogah, D. Y. *J. Am. Chem. Soc.* **1999**, *121*, 1615–1616.
(17) Di, J.; Sogah, D. Y. *Macromolecules* **2006**, *39*, 5052–5057.
(18) Beck, E.; Lokai, E.; Nissler, H. *RadTech Int. North America*; Nashville, 1996; p 160.
(19) Owusu-Adom, K.; Guymon, C. A. *Polymer* **2008**, *49*, 2636–2643.
(20) Bousmina, M. *Macromolecules* **2006**, *39*, 4259–4263.
(21) Anseth, K. S.; Wang, C. M.; Bowman, C. N. *Macromolecules* **1994**, *27*, 650–655.
(22) Tryson, G. R.; Shultz, A. R. *J. Polym. Sci., Polym. Phys. Ed.* **1979**, *17*, 2059–2075.
(23) McGrath, K. M.; Drummond, C. J. *Colloid Polym. Sci.* **1996**, *274*, 612–621.
(24) Joynes, D.; Sherrington, D. C. *Polymer* **1996**, *37*, 1453–1462.
(25) Lagaly, G.; Beneke, K. *Colloid Polym. Sci.* **1991**, *269*, 1198–1211.
(26) Katti, K. S.; Sikdar, D.; Katti, D. R.; Ghosh, P.; Verma, D. *Polymer* **2006**, *47*, 403–414.
(27) DePierro, M.; Guymon, C. A. *Macromolecules* **2006**, *39*, 617–626.
(28) Hoyle, C.; Lee, T. Y.; Roper, T. *J. Polym. Sci., Part A: Polym. Chem.* **2004**, *42*, 5301–5338.
(29) Koval', I. V. *Russ J. Org. Chem.* **2007**, *43*, 319–346.
(30) Lee, T. Y.; Caroscia, J.; Smith, Z.; Bowman, C. N. *Macromolecules* **2007**, *40*, 1473–1479.
(31) McCrum, N.; Williams, B.; Read, G. *Anelastic and Dielectric Effects in Polymeric Solids*; Dover: New York, 1991.
(32) Rao, Y.; Pochan, J. M. *Macromolecules* **2007**, *40*, 290–296.
(33) Roper, T. M.; Kwee, T.; Lee, T. Y.; Guymon, C. A.; Hoyle, C. E. *Polymer* **2004**, *45*, 2921–2929.
(34) Lester, C. L.; Smith, S. M.; Guymon, C. A. *Macromolecules* **2001**, *34*, 8587–8589.
(35) Lester, C. L.; Guymon, C. A. *Polymer* **2002**, *43*, 3707–3715.
(36) Polowinski, S. *Prog. Polym. Sci.* **2002**, *27*, 537–577.
(37) Lester, C. L.; Smith, S. M.; Jarrett, W.; Guymon, C. A. *Langmuir* **2003**, *19*, 9466–9472.
(38) Clapper, J. D.; Sievens, L.; Guymon, C. A. *Chem. Mater.* **2008**, *20*, 768–781.

MA801688Q